# Numerical Study of Stabilizer Jets Effects on Combustion Characteristics in a Jet Stabilized Combustor

Hamed Zeinivand*[1]

[1] Department of Aerospace Engineering, Sharif University of Technology.

**Abstract**

Effects of number and location of stabilizer jets on the combustion characteristics and $NO_x$ emission in a jet-stabilized combustor (JSC) have been studied numerically. It is demonstrated that an increase in axial distance of stabilizer jets from fuel injector results in $NO_x$ emission to decrease significantly and conversely thermal power of combustor enhances slightly. Also, an increase in number of jet holes (with invariable entrance air velocity) causes both the thermal power and $NO_x$ emission to enhance. As the distance between stabilizer jets and fuel injector increases from 40 mm to 60 mm and then 80 mm, uniformity of temperature profile is improved. This situation is valid for smaller number of stabilizer jets.

## Introduction

A liquid fuel gas turbine combustion chamber is a complex device where there exist numerous coupled physical and chemical phenomena, such as the fuel spray dispersion and evaporation, two-phase turbulent transport, radiation and chemical kinetics. Despite the continued advances in the gas turbine combustion technology, the challenge of improved design remains yet open in order to achieve further advancements. Modern gas turbines are currently designed with an emphasis on higher efficiency and lower emissions. In order to provide reliable design criteria along with appropriate tools to handle the modern combustion technology requirements, early detailed information of different design variants and parametric studies are necessary. For any system that is costly to build and to test, only a CFD-based analysis is capable of providing deeper insight into the transport processes encountered. In the past years, many workers have made an attempt to understand the various aspects of reactive two-phase flows. Datta and Som [1] have studied a model gas turbine combustor numerically and two-dimensionally. They have investigated the influence of fuel volatility and spray parameters on combustion performance and $NO_x$ emission. Also, the effect of pressure and swirl condition on the gas turbine performance and emission has been studied. They have concluded that the pattern factor (PF) of exit temperature distribution is reduced with a decrease in initial sauter mean diameter (SMD). Cameron et al. [2], Heitor and Whitelaw [3] and Cooper and Laurendeau [4] have performed experimental works to reveal the influence of some important parameters such as inlet swirl number, air-fuel ratio, and inlet pressure and temperature on the combustion characteristics using both gaseous and liquid fuels. Jo et al. [5] have investigated numerically the influence of inlet air temperature and equivalence ratio on spray penetration, mixing quality, subsequent burning, temperature distribution and *NOx* emission for a given $C_{10}H_{22}$ fuel in a wall jet can combustor (WJCC). They have shown that with an increase in inlet air temperature, the *NOx* level is reduced in the primary zone. Many researchers have investigated the influence of cross jets in a Rich-Burn, Quick-Mix, Lean-Burn (RQL) combustor, which was first introduced in 1980 as a strategy to reduce oxides of nitrogen and later developed in the next generation of aero-propulsion engines. In RQL combustor, cross jets are applied for quick mixing of fuel and oxidizer or for dilution of exhaust gases. Howe et al. [6] have numerically investigated the mixing characteristics of both reacting and non-reacting conditions in a configuration with simulating the quick mix region of RQL combustor. They have demonstrated that the jet-to-mainstream momentum flux ratio has a significant impact on the jet penetration depth while reaction appears to reduce the penetration depth.

The main difference between an RQL combustor and a jet-stabilized combustor (JSC) is that a wall jet in the former has an important role in the flame stabilization and there is no main swirling flow crossing over the stabilizer jets. However, in RQL combustor, cross jets have a significant role in the dilution of rich burn zone and also burning of remaining fuel in the lean burn zone such that the role of flame stabilization in this type of combustor is negligible. Accordingly, the penetration depth of jets in JSC is different from that in RQL combustor. Bauer et al. [7] have carried out various experimental measurements relating to flow behavior and temperature distribution in a jet-stabilized model combustor. Kurreck et al. [8] have then compared their numerical simulations with the measured data of Bauer et al. Bazdidi-Tehrani and Zeinivand [9] have numerically investigated JSC employing the presumed PDF model for turbulence-reaction interactions and Realizable $k$-$\varepsilon$ model for flow behavior predictions. They also have carried out an $S_n$ approximation for thermal radiation heat transfer. They have demonstrated

* Corresponding author: zeinivand@aol.com

that species and $NO_x$ predictions are in relatively good agreement with the experimental results of Bauer et al. and concluded that the thermal radiation mode plays an important part in the prediction of $NO_x$ concentration.

In the present work, the influence of number and location of stabilizer jet holes on the combustion characteristics and $NO_x$ emission regarding JSC is investigated numerically. The eddy dissipation-finite rate model is adopted to model the heat release and also to take into consideration the turbulence-reaction interactions. The present results, as much as possible, are compared with the available experimental data of Bauer et al. [7].

**General Equations and Applied Models**

Turbulent reactive flows under steady-state and incompressible conditions are governed by Favre-averaging equations, represented as in the following equations [10]:

Mass

$$\frac{\partial \widetilde{\rho}\langle u_i \rangle}{\partial x_i} = 0 \tag{1}$$

Momentum

$$\frac{\partial \widetilde{\rho}\langle u_j \rangle\langle u_i \rangle}{\partial x_i} = \frac{\partial \widetilde{\rho}\langle u_j'' u_i'' \rangle}{\partial x_i} - \frac{\partial p}{\partial x_j} + \frac{\partial \widetilde{\tau}_{ij}}{\partial x_i} + \widetilde{\rho} g_j \tag{2}$$

Energy

$$\frac{\partial \widetilde{\rho}\langle h \rangle\langle u_i \rangle}{\partial x_i} = -\frac{\partial \widetilde{\rho}\langle h'' u_i'' \rangle}{\partial x_i} + \frac{D\widetilde{p}}{Dt} - \frac{\partial \widetilde{J}_i^z}{\partial x_i} + \tau_{ij}\frac{\partial u_j}{\partial x_i} + q_i + q_r \tag{3}$$

Species

$$\frac{\partial \widetilde{\rho}\langle Y_z \rangle\langle u_i \rangle}{\partial x_i} = -\frac{\partial \widetilde{\rho}\langle Y_z'' u_i'' \rangle}{\partial x_i} - \frac{\partial \widetilde{J}_i^z}{\partial x_i} + \dot{R}_z \tag{4}$$

where, the viscous stress tensor, $\tau_{ij}$, is expressed using the following equation:

$$\tau_{ij} = \mu_t\left(\frac{\partial u_i}{\partial x_j} + \frac{\partial u_j}{\partial x_i}\right) - \frac{2}{3}\mu_t \delta_{ij}\left(\frac{\partial u_i}{\partial x_i}\right) \tag{5}$$

and the diffusive flux of chemical species, z, is defined by the Fick's law:

$$\bar{J}_i^z = -\frac{\mu_t}{Sc_k}\frac{\partial Y_z}{\partial x_i} \tag{6}$$

The generic source term, $q_i$, is modeled as in equation (7):

$$q_i = -\frac{\mu}{\Pr}\left[\frac{\partial h}{\partial x_i} + \sum_{z=1}^{N_z}\left(\frac{\Pr}{Sc_z} - 1\right)h_z\frac{\partial Y_z}{\partial x_i}\right] \tag{7}$$

The Realizable $k-\varepsilon$ turbulence model [11] is employed to model the viscous Reynolds stresses, expressed by equation (5). The motions of fuel droplets in the turbulent combustive (reactive) flow field are computed using a stochastic separated flow (SSF). The variations in mass, velocity and temperature of the droplets are acquired from the relevant conservation equation on a Lagrangian frame as expressed below.

The equation of motion for a droplet is defined as in equation (8).

$$\frac{du_{p,i}}{dt} = \frac{3}{4}C_D\frac{\mu}{\rho_p D_p^2}\left(U_i^g - u_{p,i}\right)\mathrm{Re}_p + g_i \tag{8}$$

Droplet evaporation can be estimated by solving unsteady heat and mass transfer equations for droplet, with quasi-steady descriptions of the surrounding gas field. The evaporation rate of a droplet is estimated by means of equation (9).

$$\frac{dm_p}{dt} = 2\pi d_p \rho D \ln(1+B) Nu \tag{9}$$

However, the present simulation does not take into account the effects of droplet break-up, coalescence processes and a body force such as the gravity. The Rosin-Rammler distribution with ten ranging classes from 10 to 70 μm is applied to perform the influence of air-blast atomizer. Table 1 represents the liquid fuel droplet size distribution.

Table 1. Droplet size distribution

| | |
|---|---|
| $d_{10\%}$ | 20μm |
| $d_{50\%}$ | 32μm |
| $d_{90\%}$ | 50μm |

For the combustion reaction model, a one-step global reaction model is adopted, as depicted in equation (R1).

$$C_{10}H_{22} + \frac{31}{2}O_2 \rightarrow 10CO_2 + 11H_2O \tag{R1}$$

The eddy dissipation/finite rate (ED/FR) model is applied to model the heat release and also to take into account the turbulence-reaction interactions. It computes both a chemical Arrhenius rate and a turbulent mixing rate based on the Magnussen-Hjertager [12] equation and then it chooses the lower of the two rates to be inserted into the species transport equation. The mixing reaction rates of $C_{10}H_{22}$ can be considered to be proportional to the turbulence time scale $(\varepsilon/k)$ as well as to the smallest of the fuel, oxygen, or product concentration. ED/FR model embraces an entire range of Damköhler number and it can be applied for both finite rate and infinitely fast chemistry. The mixing reaction rate for equation (R1) is then represented by:

$$R_{fu} = \rho \frac{\varepsilon}{k} \min\left\{ a Y_{fu}, a \frac{Y_{ox}}{s}, b \frac{Y_P}{1+s} \right\} \quad (10)$$

where, **s** is the stoichiometric mass ratio of oxygen to fuel and empirical constants, a and b, are equal to 4.0 and 0.5. The kinetic reaction rate for equation (R1) can be considered as:

$$\mathrm{R}_{\mathrm{kin-fuel}} = 2.58e9 \cdot \exp\left( \frac{-1.25\mathrm{e}8}{\mathrm{RT}} \right) \quad (11)$$

Hence, the lower of equations (13) and (14) determines the reaction rate of (R1).

In the present work, the thermal and prompt $NO$ formations are considered and calculated by the finite-rate chemistry. The thermal $NO$ formation rate is estimated on the basis of the extended Zeldovich mechanism as follows:

$$N_2 + O \Leftrightarrow NO + N \quad (R2)$$

$$O_2 + N \Leftrightarrow NO + O \quad (R3)$$

$$N + OH \Leftrightarrow NO + H \quad (R4)$$

where, a quasi-steady state assumption is taken on for the concentration of nitrogen atoms while The concentration, $[O]$, is given by the partial equilibrium.

A joint two-variable probability density function (PDF) in terms of temperature and oxygen concentration is employed. The mean formation rate, $S_{NO}$, can be determined by:

$$\overline{S_{NO}} = \iint S_{NO}(T, Y_{O_2}) P_1(T) P_2(Y_{O_2}) dT \, dY_{O_2} \quad (12)$$

where, the shape of $P_1(T)$ and $P_2(Y_{O_2})$ is approximated by a $\beta - PDF$.

The Discrete Ordinates method, adopting its $S_4$ approximation [13] is employed to calculate the thermal radiation. The Weighted Sum of Gray Gases Model (WSGGM) is taken on to compute the absorption coefficient with regard to the pressure, temperature and species variants.

**Geometry and Boundary Conditions**

The present model combustion chamber (reference geometry), as represented schematically by Fig. 1, is chosen consistent with the experimental setup of Bauer et al. [7]. Its diameter and length are 80 mm and 400 mm, respectively. A part of the primary air enters the combustor through four circumferential perpendicular injection jet holes as stabilizer jets of 8 mm inner diameter, 60 mm downstream of the head plate.

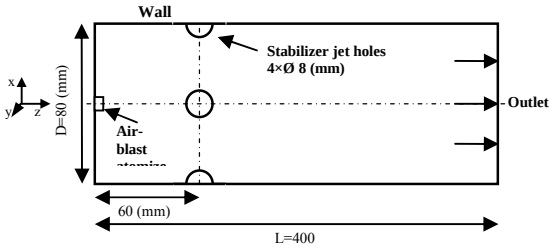


**Figure 1. Schematic view of model combustion chamber**

a first approximation for the $k$ and $\varepsilon$ may be achieved from the assumed forms as in the following equations [10]:

$$\tilde{k}_{inlet} = \frac{3}{2}\left( \left| \tilde{U}_{inlet} \right| I_t \right)^2 \quad (13)$$

$$\tilde{\varepsilon}_{inlet} = C_\mu^{3/4} \frac{\tilde{k}_{inlet}^{3/2}}{0.07 D_h} \quad (14)$$

For the radiation calculations, the walls are assumed to be gray of emissivity equal to 0.7. Further details on the present geometry, boundary conditions and fluid properties are presented in Table 2.

Table 2 Input conditions and fluid properties

| | | | |
|---|---|---|---|
| **Geometry** | | | |
| Fuel inlet zone (mm) | from r=0 to r=30 | | |
| Atomization air (mm) | from r=0.5 to r=1.5 | | |
| Jets (mm) | Diameter r=8 at z=60mm | | |
| Combustor radius (mm) | 80 | | |
| Combustor length (mm) | 400 | | |
| **Inlet boundary Conditions** | **liquid fuel** | **Atomization Air** | **Four Jets** |
| Mass flow rate (kg/h) | 1 | 1.2 | 33.5 |
| Turbulence kinetic energy ($m^2/s^2$) | --- | 39 | 6 |
| Dissipation rate of turbulence ($m^2/s^3$) | --- | 17200 | 850 |
| Temperature (K) | 295 | 295 | 295 |
| Pressure outlet (bar) | 1 | | |
| Walls | No-slip condition: u=0, v=0, w=0 | | |

**Discretization Procedure**

A Finite Volume staggered grid approach is employed to solve the governing equations including mass, momentum, energy and species in addition to the turbulence transport, fuel combustion and radiation model equations. The second-order upwind scheme is taken on for the space derivatives of the advection terms in all of the transport equations. The flow field pressure linked equations are solved using the SIMPLEC algorithm. A pressure-based algorithm, on the basis of an Eulerian-Lagrangian formulation, is applied to simulate the spray combustion.

The convergence criterion requirement is set to be $1\times10^{-6}$ for energy and about $1\times10^{-5}$ for the other terms of the transport equations. The grid spacing in the axial direction (z) is varied smoothly to reduce any fall of the accuracy of the discretization scheme, in such a way that higher concentration of nodes is allocated near the inlets, reaction zone and the walls. The influence of

mesh size on the present computations is examined extensively by considering different mesh sizes, in the range of $2.8\times10^5$ – $8\times10^5$ cells. As a typical set of results, Fig. 2 displays the independence of present results on the profiles of axial velocity at z=1.75D from mesh size. Fig. 3 shows the present temperature profiles across the combustion chamber diameter at z=1.225D. A reasonable agreement with a difference of less than 6% on average exists between the present results and the available experimental data. The temperature in the near wall region is higher than that in the central zone. The reason for this is that the core of combustor, between the axial distances of 0.07 and 0.15 (m) (i.e., between z=0.875D and z=1.875D, displays lower temperatures because of the injection of cold air jets. Also, the hot combustion products leave the primary zone through the space in between four jets without any strong mixing. At downstream, the temperature distribution becomes more uniform due to the mixing of cold flow of air through stabilizer jets and hot products of combustion.

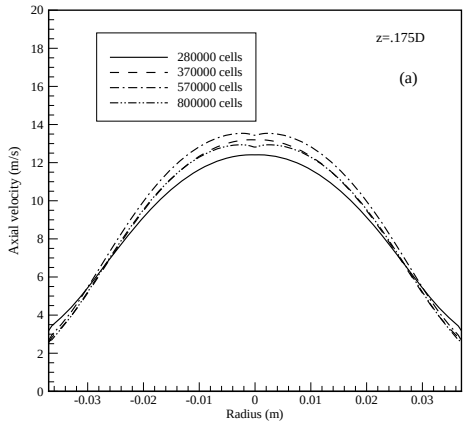


Figure 2. Independence of present computations from mesh size: axial velocity and at z=1.75D

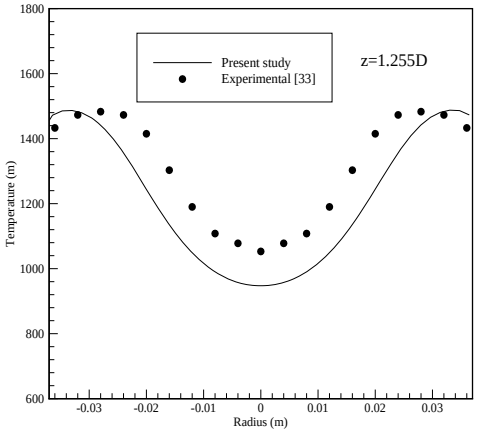


Figure 3. Profiles of temperature at z=1.225D

Fig. 4 illustrates the variations of NO pollutant concentration with axial distance along the central axis of model combustion chamber. The present predictions of NO are fairly close to the experiment. However, at the axial distance of z=075D, fresh air injected by the stabilizer jet holes reduces the NO concentration locally. In the downstream section, hot products of combustion zone (with rich NO concentration) are mixed with fresh air so that NO concentration in the rest of combustor remains constant.

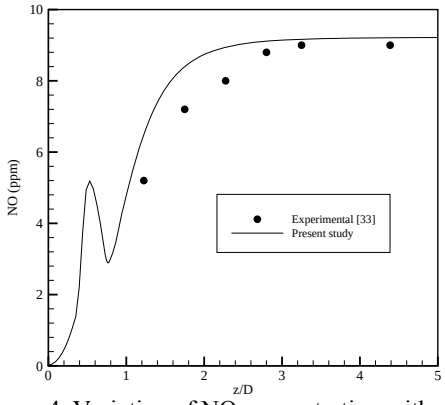


Figure 4. Variation of NO concentration with axial distance (center-line, x=y=0)

**Influence of number of stabilizer jets**

Fig.5 demonstrates the radial temperature distributions for the model combustor with 4, 6 and 8 stabilizer jet holes, at z=1.225D. An increase in the jet holes number from 4 to 6 and then 8 causes the temperature near the wall region to also increase by almost 11.2% and 18.9%, respectively. Whilst, the temperature in the central zone is decreased by nearly 7.7% and 15.3% as the jet number is raised from 4 to 6 and then 8.

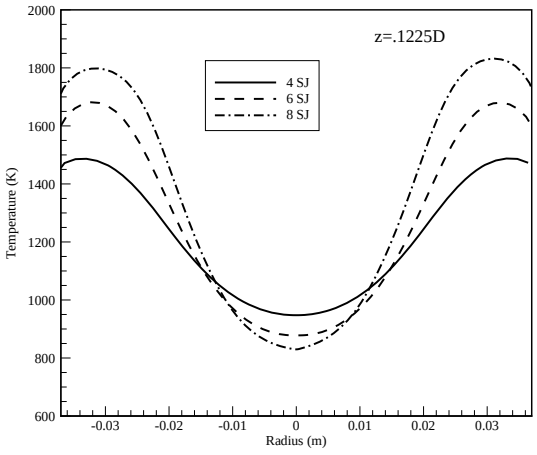


Figure 5. Influence of stabilizer jets number on temperature distribution at z=1.225D

From another point of view, as depicted by Fig. 6, with an increase of stabilizer jets number, the fraction of flow moving in the central region increases drastically and the cold flow moving toward the downstream concentrates more in the central region. At z=1.225D, the peak of axial velocity profile in the central region increases by almost 22.3% and then 38.7% as the jets number augments in turn from 4 to 6 and then 8.

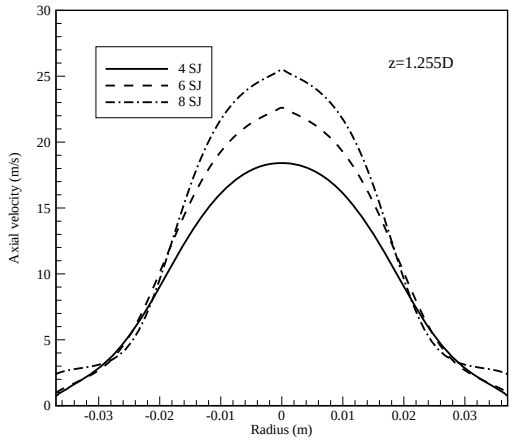


Figure 6. Influence of stabilizer jets number on velocity distribution at z=1.225D

Fig.7 illustrates the distributions of NO concentration for three different numbers of jet holes of 4, 6 and 8, at z=1.225D. Increasing the number of jets leads to an increase of *NO* concentration. This is particularly true in the near wall region where higher temperatures exist,. At z=1.225D, the maximum *NO* concentration raises from 13 to 27 (ppm) as the jets number augments from 4 to 8.

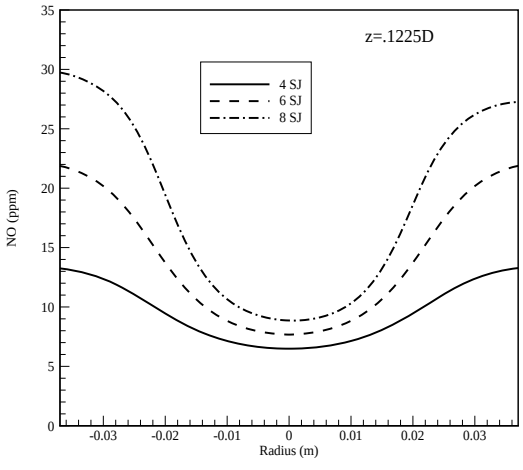


Figure 7. Effect of stabilizer jet holes number on NO concentration distribution at various axial distance

**Influence of stabilizer jets location**

Fig.8 depicts the radial temperature distributions for three different stabilizer jets locations (i.e., the distance between stabilizer jets and fuel injector) of 40, 60 and 80 (mm), at z=1.225D. The number of jet holes is kept constant at 4. At z=1.225D, as the jets position alters from 40 to 60 mm and then 80 mm the temperature of gases near the wall region of combustor rises by nearly 15% and 38%, respectively, and at the same time the temperature in the central zone decreases significantly by almost 13.5% and 50%. However, the temperature in the downstream (i.e., z/D=2.8) shows a slight decrease with an increase in the stabilizer jets position from 40 to 80 (mm). It can also be seen that as the distance between stabilizer jets and fuel injector becomes larger, the uniformity of temperature profile is improved, as compared with z=1.225D, which could lead to better conditions at the combustor's downstream section

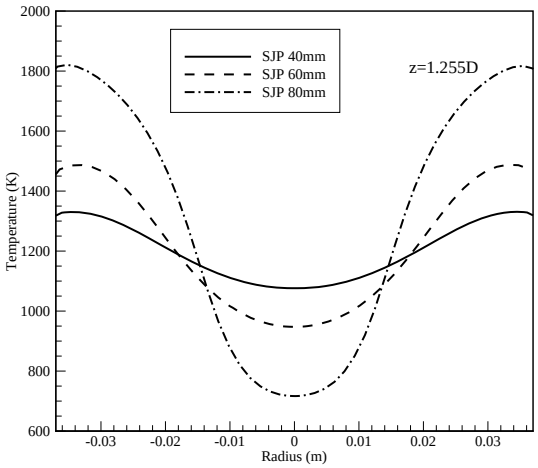


Figure 8. Influence of stabilizer jets position (SJP) on temperature distribution at z=1.225D

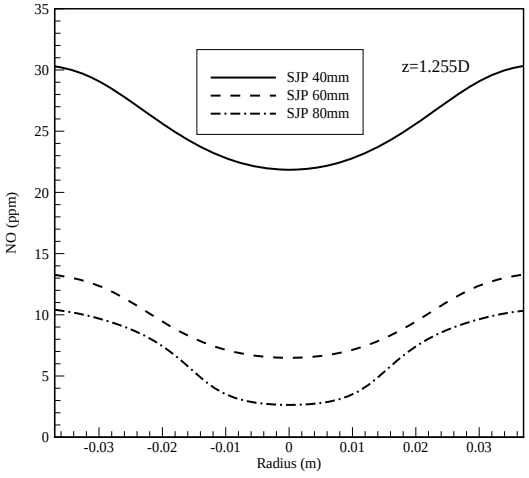


Figure 9. Effect of stabilizer jets position (SJP) on NO concentration distribution at z=1.225D

Fig.9 demonstrates the influence of stabilizer jet holes location on the NO concentration distribution, at

two values of z. As the distance between jets and fuel injector increases from 40 to 80 (mm), the NO concentration decreases significantly. For all the three jet locations under study, NO concentration has a uniform distribution in the downstream section (z=2.8). However, the NO concentration drops from about 26 (ppm) to 6 (ppm) as the jets location alters from 40 to 80 (mm).

**Conclusions**

1- As the number of stabilizer jets is raised from 4 to 6 and then 8 (with invariable entrance air velocity), the difference between the temperature of cold flow of central region and hot flow of side region becomes larger and this leads to an enhanced non-uniformity of temperature distribution towards the downstream.

2- Increasing the number of jets leads to an increase of *NO* concentration. This is particularly true in the model combustor's near wall region where higher temperatures exist.

3- In the downstream, as the stabilizer jets location is increased from 40 to 60 and then 80 (mm) the uniformity of temperature profile is improved, as compared with z=1.225D, which could lead to better conditions at the combustor's downstream section.

4- As the distance between stabilizer jets and fuel injector augments from 40 to 80 (mm), the NO concentration decreases significantly. As the distance reduces from 60 (mm) (as reference location) to 40 (mm), the NO concentration enhances by about 182% and the thermal power decreases by almost 3.5% at the combustor's exhaust.

**References**


[1] A. Datta, K.A. Som, Appl. Therm. Eng 19 (1999) 949-967.

[2] C.D. Cameron, J. Brouwer, C.P. Wood, G.S. Samuelson ASME J. Eng. Gas Turb Power 111 (1989) 31-35.

[3] M.V. Heitor, J.H. Whitelaw, Combust. Sci. Technol 64 (1986) 1-32.

[4] C.S. Cooper, N.M. Laurendeau, Proc. Combust .Inst. 28 (2000) 287-293.

[5] S. Jo, H.Y. Kim, S.S. Yoon. Num Heat Trans 54 (2008) 1101-1120.

[6] G.W. Howe, Z. Li, T.I.P, Shih, H.L. Naguyen, AIAA-91-0140, Prepared for 29th Aerospace Sci Meeting, Reno, Nevada

[7] H.J. Bauer, L. Eigenmann, S. Scherrer, S. Wittig, Int Gas Turb Aeroengine Congr Exp, Houstan, Texas, 1995.

[8] M. Kurreck, M. Willmann, S. Wittig, J Eng Gas Turb Power 120 (1998) 77-83.

[9] F. Bazdidi-Tehrani, H. Zeinivand, Energ Convers Manage 51(2010) 225-234.

[10] H.K. Versteeg, W. Malalasekera, An introduction to computational fluid dynamics: The finite volume method. Addison Wesley-Longman, 1995.

[11] T.H. Shih, W.W. Lion, A. Shabbir, Z. Yang, J. Zhu, Comput Fluids 24 (1995) 227-238.

[12] B.F. Magnussen, B.H. Hjertager, Comput Methods Appl Mech Eng 3 (1977) 269-289.

[13] R. Viskanta, M. P. Mengüc, Prog Energy Combust Sci 13 (1987) 97-160.